Measurement of the lifetimes of the $7p\ ^2P_{3/2}$ and $7p\ ^2P_{1/2}$ states of atomic cesium

George Toh,[1,2] Nathan Chalus,[3,4] Andrew Burgess,[3] Amy Damitz,[2,3] Poolad Imany,[1] Daniel E. Leaird,[1] Andrew M. Weiner,[1,2] Carol E. Tanner,[5] and D. S. Elliott[1,2,3]

[1]*School of Electrical and Computer Engineering, Purdue University, West Lafayette, Indiana 47907, USA*
[2]*Purdue Quantum Science and Engineering Institute, Purdue University, West Lafayette, Indiana 47907, USA*
[3]*Department of Physics and Astronomy, Purdue University, West Lafayette, Indiana 47907, USA*
[4]*Department of Physics, Southern Illinois University Edwardsville, Edwardsville, Illinois 62026-1654, USA*
[5]*Department of Physics, University of Notre Dame, Notre Dame, Indiana 46556, USA*

(Received 10 September 2019; published 18 November 2019)

We report time-correlated measurements of the lifetimes of the $7p\ ^2P_{3/2}$ and $7p\ ^2P_{1/2}$ states of atomic cesium. The results of these measurements are $\tau_{3/2} = 137.54\ (16)$ ns and $\tau_{1/2} = 165.21\ (19)$ ns. We use these lifetimes, together with other previously determined electric dipole matrix elements of ^{133}Cs, to determine the matrix elements $\langle 5d\ ^2D_{5/2}\|r\|7p\ ^2P_{3/2}\rangle$, $\langle 5d\ ^2D_{3/2}\|r\|7p\ ^2P_{3/2}\rangle$, and $\langle 5d\ ^2D_{3/2}\|r\|7p\ ^2P_{1/2}\rangle$. These matrix elements are in good agreement with, but of higher precision than, calculated values of these same matrix elements.

DOI: 10.1103/PhysRevA.100.052507

I. INTRODUCTION

Over the past several years, rapid progress in determining precise electric dipole (E1) matrix elements for many transitions between low-lying levels of atomic cesium has been reported [1–16]. These measurements are motivated by investigations of parity nonconservation (PNC) in cesium, which require precise determinations of these matrix elements. There is excellent agreement between E1 matrix elements calculated using powerful coupled-cluster theoretical techniques [17–20] and experimental results determined through a variety of laboratory techniques.

While most measurements of E1 matrix elements are between the ground state and an excited state, measurements of E1 elements between excited states are also needed as tests of theory. In this report we discuss our experimental measurements of the lifetimes of the $7p\ ^2P_{3/2}$ and $7p\ ^2P_{1/2}$ states of atomic cesium. The $7p\ ^2P_J$ states (where $J = 1/2$ or $3/2$) can decay spontaneously to the ground $6s\ ^2S_{1/2}$ state or the lower-lying excited $7s\ ^2S_{1/2}$ and $5d^2D_{J'}$ states (where $J' = 3/2$ or $5/2$). Since the matrix elements for two of these transitions ($\langle 7s\ ^2S_{1/2}\|r\|7p\ ^2P_J\rangle$ and $\langle 6s\ ^2S_{1/2}\|r\|7p\ ^2P_J\rangle$) have been precisely determined previously [15,16], the present lifetime measurements allow us to determine the matrix elements $\langle 5d\ ^2D_{5/2}\|r\|7p\ ^2P_{3/2}\rangle$, $\langle 5d\ ^2D_{3/2}\|r\|7p\ ^2P_{3/2}\rangle$, and $\langle 5d\ ^2D_{3/2}\|r\|7p\ ^2P_{1/2}\rangle$. While these matrix elements are not of direct relevance to atomic PNC measurements in cesium, they do provide important tests of atomic structure calculations of this heavy atom, and agreement between calculated and experimental results can improve our confidence in matrix elements that are more directly required. We report these measurements in this work. Our results are in good agreement with but of much higher precision than theoretical values [21] for these matrix elements.

II. MEASUREMENT TECHNIQUE

We use a time-correlated single-photon counting (TCSPC) technique to carry out these lifetime measurements. TCSPC, which will be described later, has been reliably used to measure the lifetimes of excited states of Cs [1,13,22,23], Fr [24–26], Rb [27,28], and BaF [29]. We use a tunable, continuous wave diode laser, gated with an acousto-optic modulator (AOM), to repetitively excite cesium atoms in a heated vapor cell. We collect and detect the fluorescence emitted through spontaneous decay and record the exponential decay of the fluorescence signal. In contrast to past measurements which use photomultipliers (PMTs) or single-photon avalanche diodes (SPADs), we use a superconducting nanowire single-photon detector (SNSPD) for photon counting. These SNSPDs have better detection efficiency and lower dark count rates compared to the previously used detectors. We discuss the SNSPD in more detail later.

We show a diagram of our experimental setup in Fig. 1. The timing sequence of the measurement is controlled by an arbitrary-wave-form generator (AWG), which generates two short electrical pulses. The first pulse controls the optical excitation of the cesium atoms, and a second pulse triggers the time correlator that measures the distribution of arrival times of the photons. The excitation lasers used are homemade external cavity diode lasers (ECDLs) tuned to wavelengths of the $6s\ ^2S_{1/2} \rightarrow 7p\ ^2P_{3/2}$ transition (455.7 nm) or the $6s\ ^2S_{1/2} \rightarrow 7p\ ^2P_{1/2}$ transition (459.4 nm), with optical powers of 10 and 20 mW, respectively. We show in Fig. 2 an energy-level diagram with the relevant states and transitions of cesium.

We chose to detect the 1.47-μm line for these measurements for several reasons: (i) We expected a reduced sensitivity to radiation trapping effects. (This expectation later proved to be incorrect, as we discuss in more detail later.) (ii) Our detection system has high efficiency at the wavelength of this transition. (iii) The branching ratio for this decay path is large, approximately 40%. (iv) The time dependence of the fluorescent decay can be simply and accurately modeled as the sum of two exponential functions, one with a known time constant (the lifetime of the $7s\ ^2S_{1/2}$ state [13]); the other yields the lifetime of the $7p\ ^2P_J$ state.

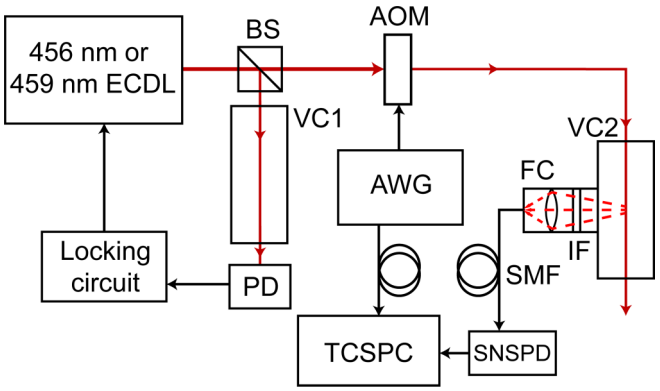

FIG. 1. Experimental layout of the $7p\,^2P_J$ lifetime measurement. An external cavity diode laser (ECDL) generates the excitation light at $\lambda = 455.7$ nm (459.4 nm) to excite the $7p\,^2P_{3/2}$ ($7p\,^2P_{1/2}$) state. The laser frequency is locked to the absorption peak using the beam splitter (BS), reference cesium vapor cell (VC1), photodiode (PD), and locking circuit. The beam passing through the primary vapor cell (VC2) is gated with an acousto-optic modulator (AOM). The arbitrary-wave-form generator (AWG) controls the timing of the measurement and sends a trigger to the time-correlated single-photon counting (TCSPC) module. The fluorescence is filtered with an interference filter (IF), coupled by a fiber collimator (FC) into a single-mode optical fiber (SMF), and detected by a superconducting nanowire single-photon detector (SNSPD).

The laser beam is split in a T90: R10 beam splitter (BS), with the reflected beam (10%) used to stabilize the laser frequency close to the peak of the Doppler-broadened absorption line. For this purpose, the beam is directed through a reference cesium cell (VC1) and onto a photodiode (PD). The PD signal is offset and fed back to the diode laser for locking to the side of the absorption peak. For the 456-nm laser, we lock to the frequency for the $6s\,^2S_{1/2}$, $F = 4 \rightarrow 7p\,^2P_{3/2}$, $F = 3, 4, 5$ transition where F is the total angular momentum

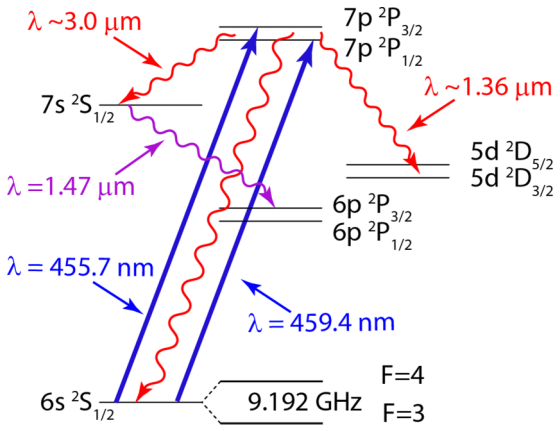

FIG. 2. Plot of the energy levels of cesium relevant to the measurements of the lifetimes of the $7p\,^2P_J$ states. We excite the $7p\,^2P_{3/2}$ ($7p\,^2P_{1/2}$) state using a diode laser tuned to 455.7 nm (459.4 nm). The $7p\,^2P_J$ state can spontaneously decay to the $6s^2S_{1/2}$ ground state or the excited $7s^2S_{1/2}$ or $5d^2D_{J'}$ states (red wavy lines). We collect the 1.47-μm fluorescence from $7s\,^2S_{1/2} \rightarrow 6p\,^2P_{3/2}$ decay (purple wavy line).

(nuclear plus electronic) of the atom. Similarly, for the 459-nm laser, we lock to the $6s\,^2S_{1/2}$, $F = 4 \rightarrow 7p\,^2P_{1/2}$, $F = 3, 4$ transition. The excited-state hyperfine splitting is not resolved in our measurements, as this splitting is less than the Doppler broadening of these peaks [30].

The primary laser beam is focused through an AOM driven at 140 MHz. The rf power that drives the AOM is pulsed on for ~330 ns at a repetition rate of 500 kHz, as controlled by the AWG. We pass the beam through three apertures along the beam path to clean up the beam shape and block the undiffracted beam from the AOM. The first-order diffracted beam from the AOM has an extinction ratio of $>500:1$, due primarily to scattered light from the undiffracted beam. We pass this beam from the AOM through the primary cesium vapor cell (VC2) for the experiment. The fluorescence to be detected is filtered using a long-pass interference filter (IF) at 1.45 μm, which blocks shorter wavelengths of fluorescence light, background light, and scattered laser light while passing only the fluorescence photons at 1.47 μm. We couple this light using a fiber collimator into a 9-μm-diameter single-mode optical fiber (SMF), angle cut to reduce the effect of reflections. This fiber also serves as a short-pass filter for wavelengths longer than ~3 μm resulting from spontaneous decay on the $7p\,^2P_J \rightarrow 7s\,^2S_{1/2}$ and $5d\,^2D_{J'} \rightarrow 6p\,^2P_{J''}$ lines.

The optical fiber, of length ~50 m, carries the photons to the detector, a Quantum Opus SNSPD. Our SNSPD operates at ~2.4 K, has a quantum efficiency of ~80% at 1.47 μm, timing jitter of 80 ps, dead time of ~25 ns, and a very low dark count rate of 100 counts/s. For highly accurate timing of the photon arrival, we use a Hydraharp 400 TCSPC module with a specified timing precision of <12 ps and 70-ns dead time. The TCSPC module measures the delay time between the start pulse from the AWG and a sync pulse from the SNSPD. The TCSPC module accumulates a histogram of the number of counts N_i vs delay time t, which we save to a computer for curve fitting.

In Fig. 3, we show an example of one such histogram for the $7p\,^2P_{3/2}$ excited state. In this plot, the ordinate represents the number of fluorescence photons N_i recorded in the ith bin over the duration of a 30-min data run, where each bin is 512 ps wide. The laser is turned on at $t \sim 120$ ns in this plot, and the fluorescence reaches a peak value of $N_i \sim 9500$ counts per bin at $t \sim 480$ ns, shortly after the time where the excitation laser is turned off. With the laser off, the fluorescence power decreases, approaching a baseline of ~100 counts.

In any counting measurement, pileup error and detector dead time can affect the total number of events registered per bin. Pileup error can result when the detector can respond to only one event within the measurement cycle. If two events occur within a single cycle, the first event is registered but the second is not. Thus, the events in later time bins are undercounted, and a correction must be applied to the data to compensate. The detection system used for the present measurement is capable of detecting and registering multiple photons within any measurement cycle, as long as they are separated by a delay time exceeding the detection dead time. As a result, it was not necessary to apply any pileup error correction to our data.

We did, however, apply a correction to minimize the effect of the dead time of the detection system. We are limited by

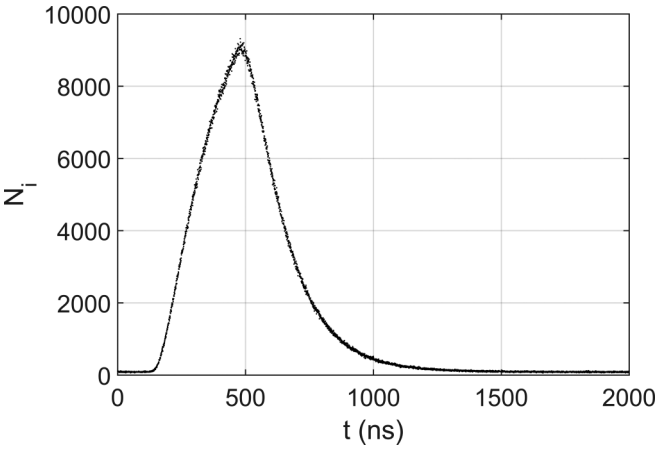

FIG. 3. Example of a full TCSPC record for one data set. The fluorescence starts to increase when the laser turns on at $t \sim 120$ ns, until it reaches a peak of ~9500 counts per bin. The number of counts decays exponentially after the laser is turned off, and we use the falling edge to determine the lifetime of the $7p\,^2P_{3/2}$ state. The low background count of ~100 counts per bin is primarily due to detector dark counts.

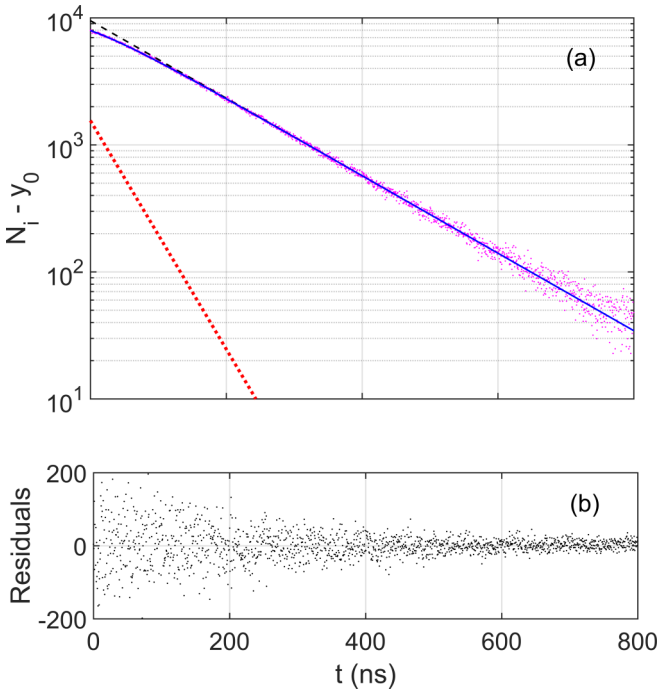

FIG. 4. A plot of one data set showing the number of counts (with background removed) $N_i - y_0$ vs delay time t. The magenta data points indicate the data, the red dotted line is $-A_{7s}\exp(-t/\tau_{7s})$, the black dashed line is $A_{7p_{3/2}}\exp[-t/\tau_{3/2}(\rho)]$, and the solid blue line is the sum of these two.

the dead time of the TCSPC module of 70 ns. To account for this dead-time error, we determined the probability P_i that a photon was received in the 70-ns period prior to the ith time bin and for each bin, multiplied the count N_i by $1 + P_i$. We compute the probability P_i by summing the total number of counts N_i in the previous 137 bins (70 ns) and dividing by the total number of cycles T_{total}/T, where $T = 2\,\mu$s is the time for one measurement cycle and T_{total} is the total collection time for one measurement. The maximum peak count rate that we used was 3.5×10^{-5} counts/bin per cycle, resulting in a maximum probability P_i of 0.005. For a typical data set, $P_i < 0.002$.

After correcting the data counts N_i for the dead-time error, we fit an exponential function of the form [22,23]

$$N_i = A_{7s}\exp\left(\frac{-t}{\tau_{7s}}\right) + A_{7p_J}\exp\left(\frac{-t}{\tau_J(\rho)}\right) + y_0, \qquad (1)$$

where $J = 1/2$ or $3/2$, to the falling edge of the data to extract the lifetimes of the $7p\,^2P_J$ states, $\tau_{1/2}(\rho)$ or $\tau_{3/2}(\rho)$, as a function of the cesium density ρ. Here, A_{7s} and A_{7p_J} are the amplitudes of the individual exponential functions, and y_0 is the background photon count due to dark counts, room lights, and excitation by incomplete laser turnoff. Typically, A_{7p_J} is 50–100 times larger than y_0.

We adjust four parameters, $\tau_J(\rho)$, A_{7s}, A_{7p_J}, and y_0, to minimize the rms deviation between the fitted curve and the data. For the lifetime τ_{7s} we use the measured value 48.28 (7) ns [13] as a fixed input parameter (the numbers in parenthesis indicate the 1σ uncertainty in the least significant digits). We show one example of a fit to the data in Fig. 4(a). The $A_{7s}\exp(-t/\tau_{7s})$ contribution, while not negligible, is small relative to the larger $A_{7p_J}\exp[-t/\tau_J(\rho)]$ term and decays away rapidly due to the short lifetime τ_{7s}. We note that A_{7s} is negative, as it can be since $\tau_{7s} < \tau_J$. The amplitude A_{7s} can be shown to be equal to $N_{7s}(0) + \tau_J\gamma_{12}N_{7p}(0)/(1 - \tau_J/\tau_{7s})$, where $N_{7s}(0)$ and $N_{7p}(0)$ are the initial populations of the $7s$ and $7p$ states, τ_{7s} and τ_J are their lifetimes, and γ_{12} is the decay rate from the $7p$ state to the $7s$ state. For $\tau_{7s} < \tau_J$, $(1 - \tau_J/\tau_{7s})$ is negative.

The residuals to these fits, shown in Fig. 4(b), computed as the difference between the individual data points and the result of the least-squares fit, show only random fluctuations about zero, with a spread consistent with shot-noise-limited detection. These residuals show no structure which if present could indicate a departure from the double exponential form of Eq. (1).

The AOM has a finite turn-off time (90%–10%), measured to be ~25 ns. Equation (1) is valid for the fluorescence decay only when the laser is completely turned off, so this leads to some ambiguity as to which time bin we should select as the start of the fit. We call this time bin the truncation time and always fit from this point to the end of the data record ($t = 2\,\mu$s). To determine the correct truncation time, we analyzed the data across a 400-ns range of truncation times. For truncation times that are too early, the data record contains time bins for which the laser was not completely off, and Eq. (1) is not a good fit. For truncation times too late, our data record is too short and the fits yield larger uncertainties. We split our data into multiple 15-ns intervals and found the interval where the fitted lifetimes $\tau_J(\rho)$ were the most uniform across all the data sets. Using this method, we found that the appropriate truncation time should be within the interval $t = 520$–535 ns for the $7p\,^2P_{1/2}$ measurements and $t = 535$–550 ns for the $7p\,^2P_{3/2}$ measurements. These truncation times differ from one another, since (i) the 456- and 459-nm laser beams are focused to slightly different locations in the AOM, and (ii) we reprogrammed the AWG between

456 and 459 data collection. Each of these changes affected the timing of the laser pulse.

For each data set, we use the mean of the fitted lifetimes within this interval as the lifetime and the standard deviation of the lifetime over the truncation interval as the truncation uncertainty. We then add the statistical uncertainty from the fit to the truncation uncertainty in quadrature to determine the uncertainty of the lifetime for each fluorescence decay curve. For most cases, the truncation uncertainty is ∼2% of the statistical uncertainty of $\tau_J(\rho)$.

III. RESULTS

We show plots of lifetime $\tau_J(\rho)$ as a function of cesium density for the $7p\,^2P_{1/2}$ and $7p\,^2P_{3/2}$ states in Fig. 5. Each data point and error bar represents the lifetime and 1σ uncertainty for one data set. Most data sets were collected for a duration of 15–30 min, with some sets collected for 2 h. The density dependence is likely due to reabsorption of 456- or 459-nm fluorescence, which increases the apparent lifetime with increasing cesium density. While this effect is similar to what is commonly referred to as radiation trapping, it differs in that the fluorescence that we detect (1.47 μm) is from a transition between two excited states of the atom and does not involve the ground state. Contrary to our expectations, our results for $\tau_{3/2}$ actually indicate a *greater* dependence on the cesium density than the lifetime measurements based upon fluorescence on the $7p\,^2P_J \rightarrow 6s\,^2S_{1/2}$ line, as reported by Campani *et al.* [31] or Pace and Atkinson [32]. We do not have a good explanation for this increased density dependence. The density dependence of the $\tau_{1/2}$ data is less than that reported in Refs. [31,32].

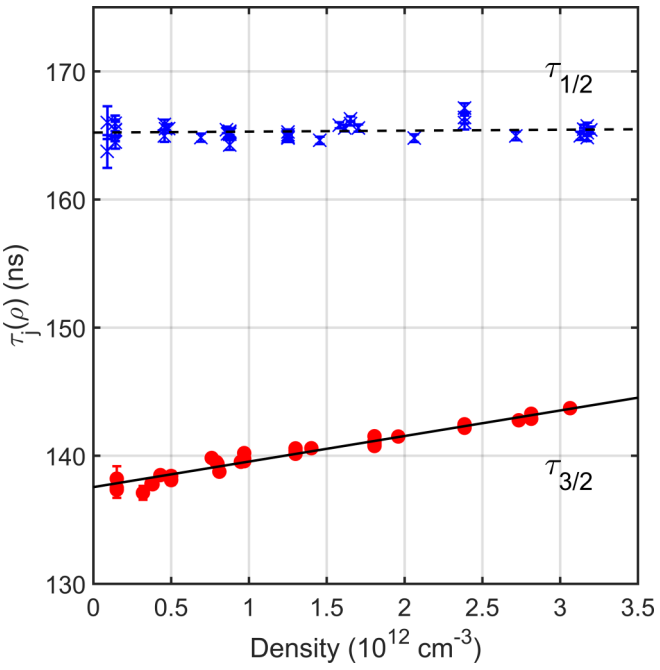

FIG. 5. Plots of lifetime $\tau_{3/2}(\rho)$ (red circles) and $\tau_{1/2}(\rho)$ (blue ×'s) vs vapor cell density. The solid (dashed) line represents the result of a linear least-squares fit to the $\tau_{3/2}$ ($\tau_{1/2}$) data. The lifetimes reported are the intercepts of the two lines.

We fit a straight line to the density-dependent plots shown in Fig. 5 to determine the intercepts, which we report as the lifetimes $\tau_{3/2} = 137.54\ (12)$ ns and $\tau_{1/2} = 165.21\ (16)$ ns. Here, the uncertainties include only statistical and truncation uncertainties. We will discuss additional uncertainties due to experimental factors in the following section. The reduced χ^2_ν of the fits were 2.3 and 2.9, respectively, indicating fluctuations among the measurements somewhat larger than the error bars of individual data points suggest. The uncertainties that we stated above for $\tau_{3/2}$ and $\tau_{1/2}$ are already expanded by a factor $\sqrt{\chi^2_\nu}$ to account for these extra fluctuations.

IV. UNCERTAINTY ANALYSIS

In order to ensure a measurement with high accuracy and precision, we investigated several potential sources of error to determine their impact on the measurement. We summarize the magnitudes of these effects in the error budget in Table I.

For a precise measurement, we require that the sensitivity of the detector and time correlator is uniform throughout the 2-μs duration of the individual record. To test for this uniformity, we recorded a number of data sets with the laser blocked, or with the laser on but the rf drive to the AOM off, allowing a weak excitation beam in the cesium cell. We fit the data N_i vs t to a straight line to determine its magnitude and slope. With the laser beam blocked, the counts from the SNSPD are due to dark counts. This measurement tests the uniformity of the TCSPC module. The slope of the fitted background signal was consistent with zero, and its magnitude allows us to estimate the effect of any nonuniformity on the lifetime τ_J. As listed in Table I, this uncertainty is at most 0.03%.

The presence of a magnetic field at the cell location can split the hyperfine components of the excited state through the Zeeman effect, leading to quantum beats in the detected fluorescence signal. To minimize this effect, we surrounded the cesium vapor cell with high-permeability material (MuMETAL) and positioned the cell such that magnetic fields in the cell were reduced to a level of <0.1 Gauss. We also tested the effect of any possible residual magnetic fields by introducing a magnetic field of 1 or 2 G for a few selected data sets. The lifetimes measured under these conditions showed no significant difference from the measurements with no applied field. From these measurements, we estimate the lifetime uncertainty due to the magnetic field to be 0.03%.

TABLE I. Error budget for the lifetimes $\tau_{1/2}$ and $\tau_{3/2}$.

	% Uncertainty	
Error	$\tau_{1/2}$	$\tau_{3/2}$
Fit uncertainty	0.10	0.09
Uniformity of sensitivity	0.03	0.03
Magnetic field	0.03	0.03
Temperature	0.01	0.05
7-s lifetime	0.02	0.02
Time calibration	0.01	0.01
Dead time	0.01	0.01
SPD jitter	0.01	0.01
Total uncertainty	0.11	0.12

We estimate that our measurement of the cell temperature is uncertain to ∼1 °C–2 °C, due to possible nonuniform heating. We measured the cell temperature with a single thermocouple probe placed close to the expected coldest point of the cell. We analyzed our density-dependent plots, such as shown in Fig. 5, with the cell temperature shifted by $\Delta T = 2\,^{\circ}\mathrm{C}$, slightly shifting the intercept of the fitted line. From this we estimate the lifetime uncertainties listed in Table I. This uncertainty for $\tau_{3/2}$ is slightly greater than that for $\tau_{1/2}$ since the density dependence of the former is larger than that of the latter, as shown in Fig. 5.

We also examined the uncertainty in τ_J due to the ±0.07-ns uncertainty in the τ_{7s} lifetime. The lifetime τ_{7s} was a fixed parameter in our fits of Eq. (1) to the data, so we determine this uncertainty by repeating the fits using values of τ_{7s} increased or decreased by its uncertainty and noted the impact on the τ_J values. This had an effect on τ_J of about 0.02%.

The time base of the TCSPC module is specified to be calibrated to ±12 ps. The ratio of this uncertainty to the lifetime τ_J gives a relative uncertainty of <0.01%.

As discussed earlier, we corrected our data for the detector and TCSPC module dead times. The resulting change in τ_J due to this correction is −0.03%. From this, we estimate an uncertainty of τ_J to be ∼0.01%.

The timing jitter in the single-photon detector is specified to be 80 ps. We calculate the effect of this jitter on the lifetime measurement as the convolution of a Gaussian distribution with the exponentially decreasing signal. In this model, the jitter has no effect on the lifetime measurement. We list this contribution in Table I as 0.01%.

We investigated the unlikely possibility of a third exponentially decaying term in Eq. (1) with a lifetime of $\tau_{5d} \sim 1.3\ \mu$s [22,23], which could be an indication that the detector registered counts related to the spontaneous decay on some other decay path from the $5d\,^2D_{5/2}$ or $5d\,^2D_{3/2}$ states. We could not observe any such signal with statistical significance.

The fiber collimator couples fluorescence from the cesium cell into the optical fiber. We estimate that the detection region, that is, the volume within the cesium cell from which fluorescence can be coupled into the optical fiber, is approximately 4 mm in diameter, larger than the 1 mm diameter of the excitation beam. This dimension is much larger than the ∼40 μm distance that thermal cesium atoms can travel in one decay lifetime. Excited atoms moving perpendicular to the laser beam are still detectable. For atoms whose motion is parallel to the laser beam, the effect of excited atoms migrating out of the detection region is largely balanced by other excited atoms migrating in. We conclude, therefore, that the effect of thermal diffusion of excited atoms out of the detection region has an insignificant impact on the lifetime measurement.

We expect that collisions with the cell wall are also not a factor in these measurements. The laser beam passes approximately through the center of the cesium cell (diameter ∼2.5 cm). Thermal atoms will travel ∼8 μs before colliding with the wall. This travel time is much greater than the lifetimes $\tau_{3/2}$ or $\tau_{1/2}$, making wall collisions unimportant.

In summary, the primary source of uncertainty in the lifetime measurement is the statistical uncertainty, with a minor contribution from the uniformity of the detector sensitivity, the residual magnetic field, and the cell temperature measurement. Adding all errors in quadrature, our final results are $\tau_{1/2} = 165.21\ (19)$ ns and $\tau_{3/2} = 137.54\ (16)$ ns.

TABLE II. Table of experimental and theoretical results.

Group	$\tau_{3/2}$ (ns)	$\tau_{1/2}$ (ns)
Experiment		
1965, Altman & Chaika [33]	250 (60)	
1967, Markova *et al.* [34]	122 (2)	
1968, Wolff & Davis [35]	111 (6)	
1969, Svanberg & Rydberg [36]	135 (1)	
1970, Schmieder *et al.* [37]	134.5 (14)	
1972, Rydberg & Svanberg [38]	135 (1)	
1975, Pace & Atkinson [32]	136 (4)	158 (5)
1976, Marek & Niemax [39]	134 (3)	158 (5)
1976, Baer & Abella [40]		147 (25)
1977, Gustavsson *et al.* [41]	136 (4)	165 (6)
1977, Deech *et al.* [42]	135 (3)	158 (3)
1978, Campani *et al.* [31]	130 (4)	150 (4)
1981, Ortiz & Campos [43]	133 (2)	155 (4)
This work	137.54 (16)	165.21 (19)
Theory		
1961, Heavens [44]	121	138
1962, Stone [45]	124	169
1981, Ortiz & Campos [43]	110	135
2016, Safronova *et al.* [21]	128 (10)	152 (18)

V. COMPARISON WITH PRIOR RESULTS

We show a summary of past experimental and theoretical results in Table II. The uncertainties of the present measurements are smaller by almost an order of magnitude than those of previous measurements. The measurements of Refs. [33,34,36–38] were carried out using level crossing techniques, Baer and Abella [40] used photon echoes, and Gustavsson *et al.* [41] used phase-modulated cw delayed coincidence. The other works [31,32,35,39,42,43] all used pulsed delayed coincidence techniques. Most of these results for $\tau_{3/2}$ are lower than ours but agree with our results to within their error bars. For $\tau_{1/2}$, we again see that most of these earlier results are lower than ours, but in this case, their results deviate from ours by more than 1σ. Overall, the phase-modulation results of Gustavsson *et al.* [41] are in closest agreement with ours.

Lifetime calculations for the $7p\,^2P_J$ states include central field approximation calculations by Heavens [44] and Stone [45], a Coulomb approximation calculation by Ortiz and Campos [43], and a coupled-cluster calculation by Safronova *et al.* [21]. The latter calculated lifetimes are in agreement with our measurements but have rather large uncertainties.

VI. MATRIX ELEMENTS

We have used our lifetime measurements to determine the E1 matrix elements $\langle 5d\,^2D_{5/2}\|r\|7p\,^2P_{3/2}\rangle$, $\langle 5d\,^2D_{3/2}\|r\|7p\,^2P_{3/2}\rangle$, and $\langle 5d\,^2D_{3/2}\|r\|7p\,^2P_{1/2}\rangle$. The $7p\,^2P_{1/2}$ state can spontaneously decay to the $6s\,^2S_{1/2}$,

$7s\,^2S_{1/2}$, and $5d\,^2D_{3/2}$ states. The E1 matrix elements for the first two of these have been precisely measured [15,16]. Using these matrix elements, we determine $\langle 5d\,^2D_{3/2}\|r\|7p\,^2P_{1/2}\rangle = 2.033\,(5)a_0$. This result is in agreement with the calculated value of $2.3\,(4)\,a_0$ [21] to within their uncertainty.

The decay of the $7p\,^2P_{3/2}$ state is not quite as clean, as there are four decay paths from this state: $6s\,^2S_{1/2}$, $7s\,^2S_{1/2}$, $5d\,^2D_{3/2}$, and $5d\,^2D_{5/2}$ states. Again, the E1 matrix elements for the first two are precisely measured, but now there are two unknown matrix elements and only a single lifetime with which to determine. We use a calculated ratio of these matrix elements $R = \langle 5d\,^2D_{5/2}\|r\|7p\,^2P_{3/2}\rangle / \langle 5d\,^2D_{3/2}\|r\|7p\,^2P_{3/2}\rangle = 2.8/0.9$, as reported by Safronova *et al.* [21], to determine $\langle 5d\,^2D_{5/2}\|r\|7p\,^2P_{3/2}\rangle = 2.480\,(8)\,a_0$ and $\langle 5d\,^2D_{3/2}\|r\|7p\,^2P_{3/2}\rangle = 0.797\,(3)\,a_0$. The uncertainties listed here do not include the uncertainty in the ratio R, which is substantial. These results agree with the calculated matrix elements [21] $\langle 5d\,^2D_{5/2}\|r\|7p\,^2P_{3/2}\rangle = 2.8\,(5)\,a_0$ and $\langle 5d\,^2D_{3/2}\|r\|7p\,^2P_{3/2}\rangle = 0.9\,(2)\,a_0$, to within their uncertainties.

VII. CONCLUSION

In conclusion, we have used time-correlated single-photon counting spectroscopy to perform measurements of the lifetimes of the cesium $7p\,^2P_{1/2}$ and $7p\,^2P_{3/2}$ excited states. The results of these measurements are $\tau_{3/2} = 137.54\,(16)$ ns and $\tau_{1/2} = 165.21\,(19)$ ns. Using these lifetime measurements, we calculate electric dipole matrix elements for the cesium $5d\,^2D_{J'} \rightarrow 7p\,^2P_J$ transitions. These lifetime measurements provide a test of theoretical methods for calculating precise models of the electronic structure of the cesium atom.

ACKNOWLEDGMENTS

This material is based upon work supported by the National Science Foundation under Grants No. PHY-1607603, No. 1839191-ECCS, and No. PHY-1852501.

[1] L. Young, W. T. Hill, S. J. Sibener, S. D. Price, C. E. Tanner, C. E. Wieman, and S. R. Leone, Precision lifetime measurements of Cs 6p $^2P_{1/2}$ and 6p $^2P_{3/2}$ levels by single-photon counting, Phys. Rev. A **50**, 2174 (1994).

[2] R. J. Rafac and C. E. Tanner, Measurement of the ratio of the cesium *D*-line transition strengths, Phys. Rev. A **58**, 1087 (1998).

[3] R. J. Rafac, C. E. Tanner, A. E. Livingston, and H. G. Berry, Fast-beam laser lifetime measurements of the cesium $6p^2P_{1/2,3/2}$ states, Phys. Rev. A **60**, 3648 (1999).

[4] A. Derevianko and S. G. Porsev, Determination of lifetimes of $6P_J$ levels and ground-state polarizability of Cs from the van der Waals coefficient C_6, Phys. Rev. A **65**, 053403 (2002).

[5] J. M. Amini and H. Gould, High Precision Measurement of the Static Dipole Polarizability of Cesium, Phys. Rev. Lett. **91**, 153001 (2003).

[6] N. Bouloufa, A. Crubellier, and O. Dulieu, Reexamination of the 0_g^- pure long-range state of Cs_2: Prediction of missing levels in the photoassociation spectrum, Phys. Rev. A **75**, 052501 (2007).

[7] Y. Zhang, J. Ma, J. Wu, L. Wang, L. Xiao, and S. Jia, Experimental observation of the lowest levels in the photoassociation spectroscopy of the 0_g^- purely long-range state of Cs_2, Phys. Rev. A **87**, 030503(R) (2013).

[8] B. M. Patterson, J. F. Sell, T. Ehrenreich, M. A. Gearba, G. M. Brooke, J. Scoville, and R. J. Knize, Lifetime measurement of the cesium $6P_{3/2}$ level using ultrafast pump-probe laser pulses, Phys. Rev. A **91**, 012506 (2015).

[9] M. D. Gregoire, I. Hromada, W. F. Holmgren, R. Trubko, and A. D. Cronin, Measurements of the ground-state polarizabilities of Cs, Rb, and K using atom interferometry, Phys. Rev. A **92**, 052513 (2015).

[10] C. E. Tanner, A. E. Livingston, R. J. Rafac, F. G. Serpa, K. W. Kukla, H. G. Berry, L. Young, and C. A. Kurtz, Measurement of the $6p\,^2P_{3/2}$ State Lifetime in Atomic Cesium, Phys. Rev. Lett. **69**, 2765 (1992).

[11] J. F. Sell, B. M. Patterson, T. Ehrenreich, G. Brooke, J. Scoville, and R. J. Knize, Lifetime measurement of the cesium $6P_{3/2}$ state using ultrafast laser-pulse excitation and ionization, Phys. Rev. A **84**, 010501(R) (2011).

[12] S. C. Bennett, J. L. Roberts, and C. E. Wieman, Measurement of the dc Stark shift of the $6S \rightarrow 7S$ transition in atomic cesium, Phys. Rev. A **59**, R16(R) (1999).

[13] G. Toh, J. A. Jaramillo-Villegas, N. Glotzbach, J. Quirk, I. C. Stevenson, J. Choi, A. M. Weiner, and D. S. Elliott, Measurement of the lifetime of the $7s^2S_{1/2}$ state in atomic cesium using asynchronous gated detection, Phys. Rev. A **97**, 052507 (2018).

[14] G. Toh, A. Damitz, N. Glotzbach, J. Quirk, I. C. Stevenson, J. Choi, M. S. Safronova, and D. S. Elliott, Electric dipole matrix elements for the $6p^2P_J \rightarrow 7s^2S_{1/2}$ transition in atomic cesium, Phys. Rev. A **99**, 032504 (2019).

[15] A. Damitz, G. Toh, E. Putney, C. E. Tanner, and D. S. Elliott, Measurement of the radial matrix elements for the $6s^2S_{1/2} \rightarrow 7p^2P_J$ transitions in cesium, Phys. Rev. A **99**, 062510 (2019).

[16] G. Toh, A. Damitz, C. E. Tanner, W. R. Johnson, and D. S. Elliott, Determination of the Scalar and Vector Polarizabilities of the Cesium $6s^2S_{1/2} \rightarrow 7s^2S_{1/2}$ Transition and Implications for Atomic Parity Nonconservation, Phys. Rev. Lett. **123**, 073002 (2019).

[17] M. S. Safronova, W. R. Johnson, and A. Derevianko, Relativistic many-body calculations of energy levels, hyperfine constants, electric-dipole matrix elements, and static polarizabilities for alkali-metal atoms, Phys. Rev. A **60**, 4476 (1999).

[18] V. A. Dzuba, V. V. Flambaum, and J. S. M. Ginges, Calculations of parity-nonconserving $s-d$ amplitudes in Cs, Fr, Ba^+, and Ra^+, Phys. Rev. A **63**, 062101 (2001).

[19] V. A. Dzuba, V. V. Flambaum, and J. S. M. Ginges, High-precision calculation of parity nonconservation in cesium and test of the standard model, Phys. Rev. D **66**, 076013 (2002).

[20] S. G. Porsev, K. Beloy, and A. Derevianko, Precision determination of weak charge of ^{133}Cs from atomic parity violation, Phys. Rev. D **82**, 036008 (2010).

[21] M. S. Safronova, U. I. Safronova, and C. W. Clark, Magic wavelengths, matrix elements, polarizabilities, and lifetimes of Cs, Phys. Rev. A **94**, 012505 (2016).

[22] B. Hoeling, J. R. Yeh, T. Takekoshi, and R. J. Knize, Measurement of the lifetime of the atomic cesium $5^2D_{5/2}$ state with diode-laser excitation, Opt. Lett. **21**, 74 (1996).

[23] D. DiBerardino, C. E. Tanner, and A. Sieradzan, Lifetime measurements of cesium $5d^2D_{5/2,3/2}$ and $11s^2S_{1/2}$ states using pulsed-laser excitation, Phys. Rev. A **57**, 4204 (1998).

[24] W. Z. Zhao, J. E. Simsarian, L. A. Orozco, W. Shi, and G. D. Sprouse, Measurement of the $7p^2P_{3/2}$ Level Lifetime in Atomic Francium, Phys. Rev. Lett. **78**, 4169 (1997).

[25] J. E. Simsarian, L. A. Orozco, G. D. Sprouse, and W. Z. Zhao, Lifetime measurements of the $7p$ levels of atomic francium, Phys. Rev. A **57**, 2448 (1998).

[26] E. Gomez, L. A. Orozco, A. Perez Galvan, and G. D. Sprouse, Lifetime measurement of the $8s$ level in francium, Phys. Rev. A **71**, 062504 (2005).

[27] D. Sheng, A. Pérez Galván, and L. A. Orozco, Lifetime measurements of the $5d$ states of rubidium, Phys. Rev. A **78**, 062506 (2008).

[28] E. Gomez, F. Baumer, A. D. Lange, G. D. Sprouse, and L. A. Orozco, Lifetime measurement of the $6s$ level of rubidium, Phys. Rev. A **72**, 012502 (2005).

[29] P. Aggarwal, V. Marshall, H. Bethlem, A. Boeschoten, A. Borschevsky, M. Denis, K. Esajas, Y. Hao, S. Hoekstra, K. Jungmann *et al.*, Lifetime measurements of the $A^2\Pi_{1/2}$ and $A^2\Pi_{3/2}$ states in BaF, arXiv:1907.06879.

[30] W. Williams, M. Herd, and W. Hawkins, Spectroscopic study of the $7p_{1/2}$ and $7p_{3/2}$ states in cesium-133, Laser Phys. Lett. **15**, 095702 (2018).

[31] E. Campani, G. Degan, and G. Gobini, Direct measurement of $7P_{1/2}$, $7P_{3/2}$ lifetimes in cesium, Lett. Nuovo Cimento **23**, 187 (1978).

[32] P. W. Pace and J. B. Atkinson, The lifetimes of the $7^2P_{1/2}$ and $7^2P_{3/2}$ states of cesium, Can. J. Phys. **53**, 937 (1975).

[33] E. L. Altman and M. P. Chaika, Determination of the lifetime of the excited $7p^2P_{3/2}$ state of cesium from double resonance experiments, Opt. Spectrosc. **19**, 538 (1965).

[34] G. Markova, G. Khvostenko, and M. Chaika, Lifetime of the $6^2P_{3/2}$ and $7^2P_{3/2}$ states of Cesium, Opt. Spectrosc. **23**, 456 (1967).

[35] R. J. Wolff and S. P. Davis, Direct measurement of atomic lifetimes of cesium and sodium, J. Opt. Soc. Am. **58**, 490 (1968).

[36] S. Svanberg and S. Rydberg, Level crossing investigation of the $6p^2P_{3/2}$ and $7p^2P_{3/2}$ levels of Cs^{133}, Cs^{135}, and Cs^{137}, Z. Phys. A: Hadrons Nucl. **227**, 216 (1969).

[37] R. W. Schmieder, A. Lurio, W. Happer, and A. Khadjavi, Level-crossing measurement of lifetime and hfs constants of the $^2P_{3/2}$ states of the stable alkali atoms, Phys. Rev. A **2**, 1216 (1970).

[38] S. Rydberg and S. Svanberg, Investigation of the np $^2P_{3/2}$ level sequence in the Cs I spectrum by level crossing spectroscopy, Phys. Scr. **5**, 209 (1972).

[39] J. Marek and K. Niemax, The influence of collisions of Xe atoms on the lifetime of atomic states of Cs, J. Phys. B: At. Mol. Phys. **9**, L483 (1976).

[40] T. Baer and I. Abella, Photon echoes on the $6S \rightarrow 7P$ transitions in Cs vapor, Phys. Lett. A **59**, 371 (1976).

[41] M. Gustavsson, H. Lundberg, and S. Svanberg, An efficient method for measuring atomic and molecular lifetimes using a modulated or deflected cw dye laser beam, Phys. Lett. A **64**, 289 (1977).

[42] J. S. Deech, R. Luypaert, L. R. Pendrill, and G. W. Series, Lifetimes, depopulation cross sections and hyperfine structures of some Rydberg S and D states of ^{133}Cs, J. Phys. B: At. Mol. Phys. **10**, L137 (1977).

[43] M. Ortiz and J. Campos, Lifetime measurements of 7P levels of Cs(I) by means of laser excitation, J. Quant. Spectrosc. Radiat. Transfer **26**, 107 (1981).

[44] O. S. Heavens, Radiative transition probabilities of the lower excited states of the alkali metals, J. Opt. Soc. Am. **51**, 1058 (1961).

[45] P. M. Stone, Cesium oscillator strengths, Phys. Rev. **127**, 1151 (1962).